



Sharif University of Technology

Scientia Iranica

Transactions A: Civil Engineering

www.scientiairanica.com



Research Note

A comparative study on the ductility and energy dissipation capacity of SMRF and V-EBF systems

S. Pourzeynali* and A. Shakeri

Department of Civil Engineering, University of Guilan, Rasht, Iran.

Received 10 September 2013; received in revised form 17 May 2014; accepted 25 January 2015

KEYWORDS

SMRF;
V-EBF;
Vertical shear link;
Ductility;
Energy dissipation;
Earthquake;
Seismic performance;
Finite element analysis;
Cyclic loading.

Abstract. Special Moment Resisting Frames (SMRF) are one of the most well-known and practical Seismic Force Resisting Systems (SFRSs), with a high range of ductility and energy dissipation, as well as the capability of providing enough space for the architectural design purpose of buildings or other structures. One of the most important deficiencies of this system is the matter of controlling its maximum drift against the lateral force of earthquakes, which results in a non-economical design, especially in tall buildings. Eccentrically Braced Frame with Vertical link beam (V-EBF) is almost a new seismic force resisting system in which the vertical link beam has the role of the ductile member with a wide range of ductility and energy dissipation capacity. In this paper, the ductility and energy dissipation capacity of the SMRF and V-EBF systems are compared. For this purpose, a number of one-story, one-bay frames, including these two systems, with different characteristics, are analyzed using the non-linear finite element method under quasi-static cyclic loading, and the results are compared.

© 2015 Sharif University of Technology. All rights reserved.

1. Introduction

Selection of an adequate Seismic Force Resisting System (SFRS) is one of the most important tasks in the design of structures. Steel structures in seismic areas are expected to produce enough stiffness, energy dissipation, and ductility. Stiffness should be provided in order to control the maximum amount of lateral displacement, which may cause the destruction of non-structural parts of the structure. Energy dissipation is required for dissipating the inserted energy of the earthquake, and a sufficient amount of ductility is needed to reduce the base shear applied to structures during earthquakes.

The Eccentrically Braced Frame (EBF) has been

investigated in a number of research works showing the ability of this system in providing a significant amount of ductility and energy dissipation [1-5]. Berman and Bruneau [6-9] conducted experimental and analytical research on the application of links with tubular sections after which the use of these sections as the links in the EBF is permitted by AISC seismic provisions [10]. One of the most novel types of these systems is the Eccentrically Braced Frame with a Vertical link beam (V-EBF) in which a vertical link is used as a fuse that has the role of energy dissipation of the system by sustaining large plastic deformation, while the beam, braces and columns remain in the elastic region. This performance causes the whole system, except the vertical link, to remain undamaged during the earthquake and, if so, to be easily replaced by exchanging the destroyed link with a new one.

Lack of knowledge about its performance is one of the main problems in utilizing this system, although some research has been undertaken in this regard.

*. Corresponding author. Mobile: +98 911 3310919;

Fax: +98 13 33690271

E-mail addresses: pourzeynali@guilan.ac.ir (S.

Pourzeynali); ashkan.shakeri@gmail.com (A. Shakeri)

Wakabayashi [11] studied the hysteresis performance of a chevron Centrally Braced Frame (CBF) and an Eccentrically Braced Frame with a Vertical link (V-EBF). The results show that the V-EBF system has a more stable hysteresis curve, more ductility, and more capacity of energy dissipation in comparison with that of the CBF system. Fehling and his co-workers [12] did some research into vertical shear links. In this research, a vertical shear link was designed without lateral bracing, and a finite element study was performed to find out more about the requirements of lateral bracing in the lower end of these links. Astaneh-Asl [13,14] worked on the effects of gusset plate eccentricities in inverted-chevron braces, on their ductility. The specimen, with vertical eccentricity in its gusset plate, showed the most ductility and the most stable hysteresis curves. Sarraf and Bruneau [15-17] conducted some research into the utilization of vertical shear link, named the Shear Panel System (SPS), in seismic rehabilitation of Deck-Truss bridges. In that research, two other types of damping system, EBF and TADAS, also were studied. The results showed that all three damping devices had significant effects on enhancement of the seismic performance of these bridges. Zahrai and Bruneau [18,19] also tried to utilize EBF, SPS and TADAS systems to retrofit some bridges with different bay lengths. In order to rehabilitate these structures, ADINA [20] and DRAIN-2DX [21] softwares were utilized. In that research, it was shown that the shear panels (vertical links) provided the required ductility and energy dissipation, by sustaining large plastic deformations, while the other structural components were in the elastic region.

In the present study, the performance of a V-EBF system is compared with that of a special moment resisting system, which is well-known for its high range of ductility and energy dissipation. For this purpose, first, samples of these two systems are designed, based on AISC 2010 seismic provisions [10]. Then, nonlinear finite element analyses are performed by ABAQUS [22] software and, finally, the results are compared from a ductility and energy dissipation point of view.

2. Design of the systems

All specimens (V-EBFs and SMRFs) studied in this research are designed according to AISC provisions, including seismic provisions [10], prequalified connections [23] and specifications [24]. Then, these samples are simulated in ABAQUS software [22], and analyzed under quasi-static loading, according to SAC-ATC 24 [25] loading protocol.

2.1. Design of V-EBF systems

According to AISC 2010 seismic provisions [10], for shear yielding links, the link length (e) shall be limited

by the following relationship:

$$e < 1.6(M_p/V_p), \quad (1)$$

where M_p and V_p are the plastic moment and shear strength of the link section, respectively. M_p can be obtained by the following equations [10]:

$$M_p = F_y * Z \quad \text{for} \quad P_r/P_c \leq 0.15, \quad (2)$$

$$M_p = F_y * Z [(1 - P_r/P_c)/0.85] \quad \text{for} \quad P_r/P_c \geq 0.15, \quad (3)$$

where F_y , Z , P_r , and P_c are the yield stress, plastic section modulus, required axial strength and nominal axial yield strength of the link beam, respectively. V_p also can be evaluated as follows [10]:

$$V_p = 0.6F_y * A_{lw} \quad \text{for} \quad P_r/P_c \leq 0.15, \quad (4)$$

$$V_p = 0.6F_y * A_{lw} \sqrt{[1 - (P_r/P_c)^2]} \quad \text{for} \quad P_r/P_c \geq 0.15, \quad (5)$$

where A_{lw} , for the case of I-shaped link sections, can be calculated by Eq. (6) [10]:

$$A_{lw} = (d - 2t_f) * t_w, \quad (6)$$

where d , t_f , and t_w are the height, the flange thickness and the web thickness of the link beam. In the present study, I-shaped sections, namely: IPE200 and IPB160, are used as the link beam. According to the above statements for shear yielding links, the link length (e) shall be less than 54.7 (cm) for IPE200 links, and less than 80.4 cm for IPB160 links. So, in this investigation, in order to study the effect of link length on the performance of a V-EBF system, four lengths of 20, 30, 40, and 50 centimeters are chosen for both the above mentioned I-shaped sections. The maximum amount of distance between the link stiffeners (a_{\max}) of the shear links, which are expected to undergo a rotation amount of, at least 0.08 Radians, can be calculated by Eq. (7) [10]:

$$a_{\max} = 30t_w - d/5, \quad (7)$$

where t_w and d are described earlier. For IPE 200 and IPB 160 sections, these values are equal to 12.8 (cm) and 20.8 (cm), respectively. For simplicity, for each link length, the distances between the link stiffeners are chosen as 10 cm for IPE 200 sections, and for IPB160. However, for considering the effect of distance between the link stiffeners, two types of distance are selected: the first type with the maximum available distance ($a \leq a_{\max}$) and the second type with $a = 10$ cm (the minimum available distance between stiffeners considering constructional issues). The other parts of the V-EBF frames (the beam, braces and columns) are designed based on the plastic shear of the vertical link,

Table 1. Summary of link properties.

Section type	M_p (kg.cm)	V_p (kg)	e_{maximum} (cm)	a_{maximum} (cm)
IPE200	504552	14757.12	54.7	12.8
IPB160	775921.1	15436.8	80.42	20.8

in such a way that they will remain elastic during the large deformations of the link beam. It is important to specify that the values of plastic shear for IPE 200 and IPB 160 sections are almost the same. Table 1 summarizes the material type, the amounts of M_p , V_p , e_{maximum} , and a_{maximum} . It should be expressed that all components of all specimens, either V-EBFs or SMRFs, are constructed of ST37 steel material. To simplify its modeling in ABAQUS software, Young's modulus of elasticity, yield stress, ultimate stress, and Poisson's ratio of this material (ST37) are selected as 2.1×10^6 (kg/cm²), 2400 (kg/cm²), 3700 (kg/cm²) and 0.3, respectively.

2.2. Design of SMRF systems

According to AISC seismic provisions [10], there are six types of moment resisting constructions prequalified to be used in SMRF systems. Reduced Beam Section (RBS) moment resisting connection is one of the most ductile one among these prequalified moment connections. Details of the RBS radius-cut are shown in Figure 1.

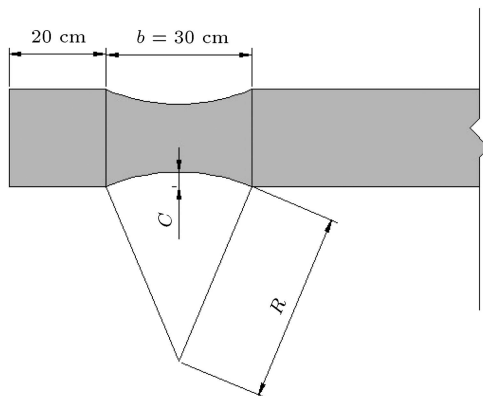
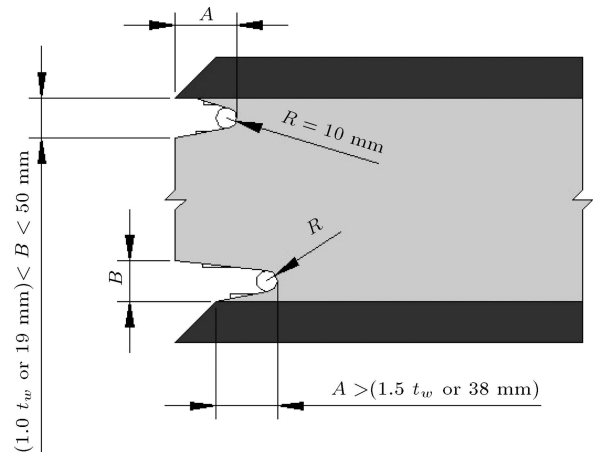
The values of parameters a , b , and c (stated in Figure 1) are limited by the following equations [23]:

$$0.5b_f \leq a \leq 0.75b_f, \quad (8)$$

$$0.65d \leq b \leq 0.85d, \quad (9)$$

$$0.1b_f \leq c \leq 0.25b_f, \quad (10)$$

where b_f and d are the flange width and the depth of the beam, respectively. According to the above statements, in this paper, in which the IPB240 section is used as the beam for the SMRFs, a and b

**Figure 1.** Details of the RBS.**Figure 2.** Details of the weld access hole.

parameters are selected equal to 15 and 20 centimeters, respectively. In order to investigate the effect of depth of RBS-cut on the performance of the SMRF system, values of the c parameter (depth of RBS-cut) are chosen as 10%, 15%, 20%, and 25% of the beam flange width, which are equal to 2.4, 3.6, 4.8, and 6 centimeters, respectively. The amount of R can be calculated by the following relation [23]:

$$R = (4c^2 + b^2)/(8c). \quad (11)$$

Details of the weld access hole are presented in Figure 2. For the IPB 240 profile, which is used for the beam, the amounts of A and B are chosen as 25 and 20 millimeters, respectively.

According to the standard of prequalified connections [23], the clear span-to-depth ratio of the beam should be equal to 7 or greater for SMRFs. For the purpose of investigating the effect of the amount of this ratio on the performance of the SMRFs system, three values of 7, 12 and 20 are selected to be used in this paper.

2.3. Model properties

According to the above demonstrations, for the purpose of comparing the ductility and energy dissipation of V-EBF and SMRF systems, twelve models of the V-EBF system (Figure 3), containing four samples constructed of IPE 200 and eight samples constructed of IPB 160 as link beam sections, as well as twelve models of the SMRF system constructed of two columns of IPB 320 with 330 cm height, and a beam of IPB 240 containing three groups with different amounts of clear span-to-beam depths are studied in ABAQUS software. Details are presented in Tables 2 and 3, respectively.

3. Finite element modeling

3.1. Element selection

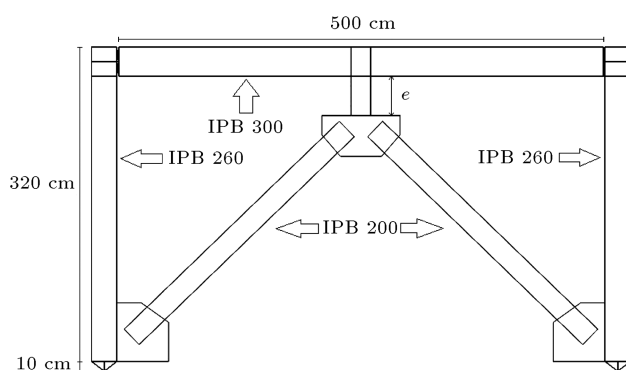
In order to compare the seismic performance of the above seismic force resisting systems, it is required

Table 2. Properties of V-EBF models considered in this study.

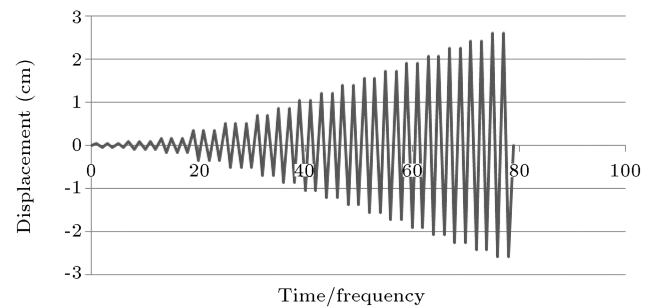
Sample	Link beam section	Link length (cm)	No. of stiffeners	Column	Beam	Brace
S-1	IPE200	20	1	IPB260	IPB300	IPB200
S-2		30	2			
S-3		40	3			
S-4		50	4			
S-5	IPB160	20	0			
S-6		20	1			
S-7		30	1			
S-8		30	2			
S-9		40	1			
S-10		40	3			
S-11		50	2			
S-12		50	4			

Table 3. Properties of SMRF models considered in this study.

Sample	C/b_f (%)	L (cm)	d_f	L/d_f
S-7-1	10%	168	24	7
S-7-2	15%			
S-7-3	20%			
S-7-4	25%			
S-12-1	10%	288	24	12
S-12-2	15%			
S-12-3	20%			
S-12-4	25%			
S-20-1	10%	480	24	20
S-20-2	15%			
S-20-3	20%			
S-20-4	25%			

**Figure 3.** Typical eccentrically braced frame with vertical link beam (V-EBF).

to model them using a finite element software for which ABAQUS software is chosen (as stated earlier). In this software, since use of solid elements would cause a heavy computational job for the computing machine to reduce process time, a 4-node shell element

**Figure 4.** Loading pattern used for V-EBF systems.

with reduced integral (S4R) is utilized for the simulations.

3.2. Loading pattern

The quasi-static cyclic loading suggested by SAC-ATC 24 [25] is used for the analysis. According to this loading protocol, two steps are required to find the suitable load pattern. In the first step, a ramped static displacement is applied to the structure and, from the resulting force-displacement diagram, the displacement of the yield point (Δ_y) will be found. In the second step, by multiplying some coefficients (represented by the provision) to the Δ_y value, the amount of applied displacement in each cycle will be calculated. In this way, the cyclic loading diagrams for V-EBF and SMRF systems that apply to the upper level of these frames are found as illustrated in Figures 4 and 5, respectively.

3.3. Validation and verification

In order to validate the analysis results of ABAQUS software used in this study, the "experimental investigation of tubular links for eccentrically braced frames" conducted by Berman and Bruneau [7] is re-simulated in this software. The steel material used in the experiment study of reference [7] was A572 Gr. 50 ($F_y = 345$ MPa), and the quasi-static loading protocol

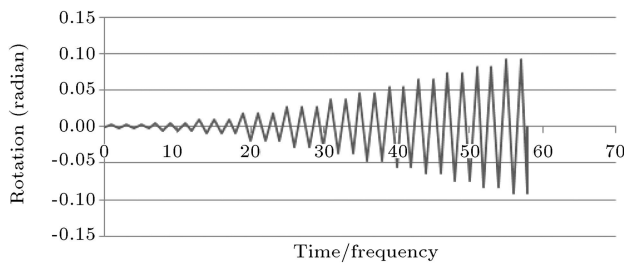


Figure 5. Loading pattern used for SMRF systems.

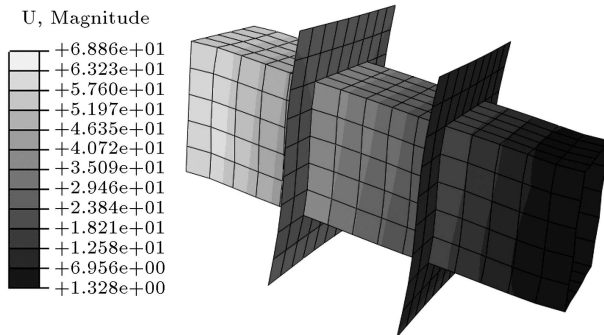


Figure 6. Deformed link model.

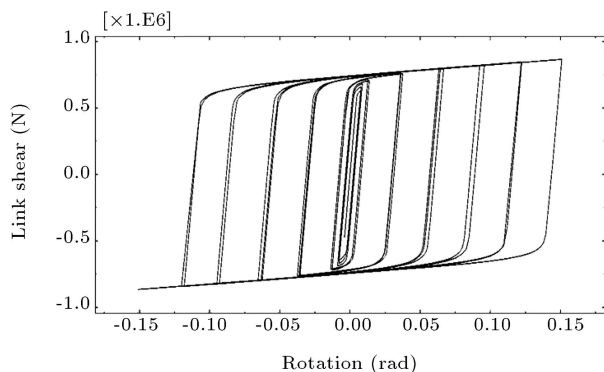


Figure 7. Analytical hysteresis curve (ABAQUS result).

used in the experiment was based on the provisions demonstrated by SAC-ATC 24 [25], as used in this study. The S4R element (described previously) is used in modeling of the link beam by ABAQUS. The deformed model of the link and the hysteresis diagram resulted from the finite element analysis are presented in Figures 6 and 7, respectively. Comparing these figures with Figures 8 and 9 in the research of Berman and Bruneau [7], it is observed that the results obtained from the finite element analysis of ABAQUS, used in this investigation, has an acceptable conformity with experimental results.

4. Results obtained from analysis of the models

4.1. Von Mises stress contours

Von Mises stress contours of the V-EBF models, S1 and S4 (with minimum and maximum lengths of IPE

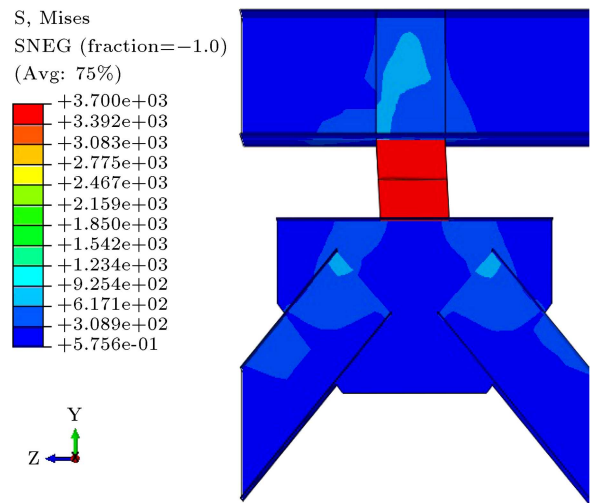


Figure 8. Von Mises stress distribution in S1 model.

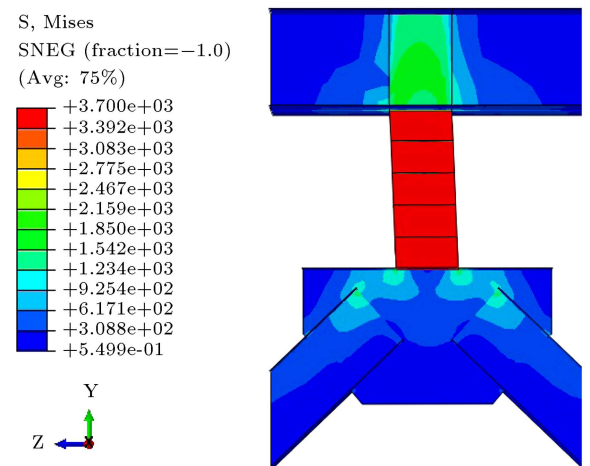


Figure 9. Von Mises stress distribution in S4 model.

link sections, respectively), as examples, are presented in Figures 8 and 9, respectively. It can clearly be seen that the shear link webs yield due to shear force. In addition, it is observed that the increase in the amount of shear link length results in an increase in the value of the stress in the beam web panel zone. This is because of the augmentation of the amount of concentrated moment applied to the beam web panel zone.

Von Mises stress contours of models S5 and S6 (with IPB link sections), as another example of V-EBF specimens, are shown in Figures 10 and 11, respectively. It is observed that although the link lengths in these two models are the same (equal to 20 cm), specimen S8, with 2 link stiffeners, grasps more value of concentrated stress in the beam web panel zone than specimen S9, which has 1 stiffener. So, it is found that in addition to the increase in link length (which is discussed earlier), the increase in the number of link stiffeners also results in an increase in the stress value in the panel zone of the beam. This is because augmentation of the link stiffeners leads to an increase

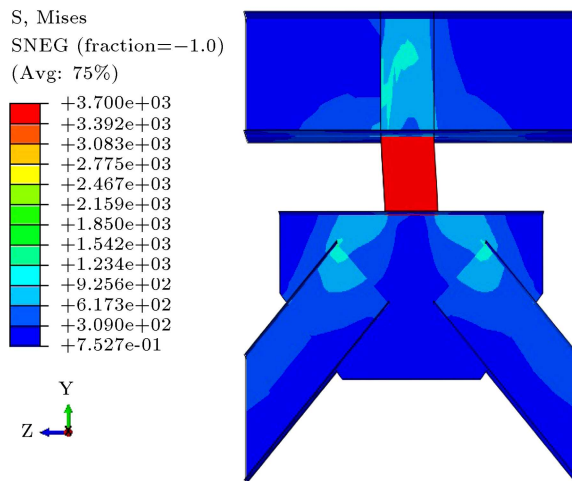


Figure 10. Von Mises stress distribution in S5 model.

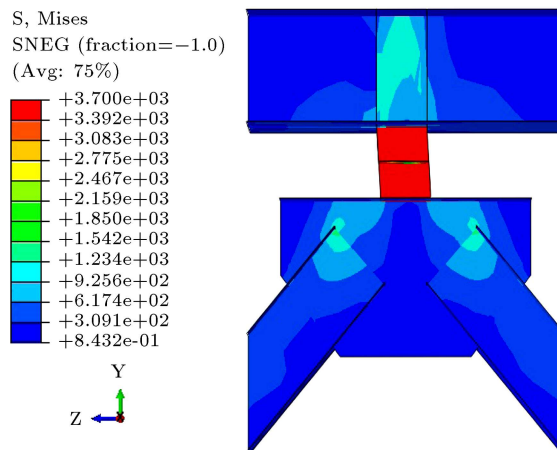


Figure 11. Von Mises stress distribution in S6 model.

in the amount of link stiffness, and the shear force which applies to the beam web.

Figure 12 shows the maximum amounts of Von Mises stress in the beam panel zones of the V-EBF specimens. The models are classified in three groups: Specimens with IPE 200 link sections (IPE), specimens with IPB 160 and maximum amounts of distance between the link stiffeners (IPB-a), and specimens with IPB 160 and with stiffener distance of 10 cm (IPB-b). It can be clearly seen that the above statements are approved by this diagram. In addition, it is observed that the first group (with IPE link sections), applies lower stress to the panel zones in comparison with the two other groups of specimens (with IPB link sections).

Von Mises stress contours of the SMRF models, S-7-1 and S-7-4, (with minimum and maximum amounts of RBS-cut, respectively), as examples of the first group of SMRF specimens (with span-to-beam depth ratio equals to 7), are presented in Figures 13 and 14. It can be seen that an increase in the amount of RBS-cut (c parameter) leads to an increase in the Von Mises stress in the weakened section point and a reduction in the

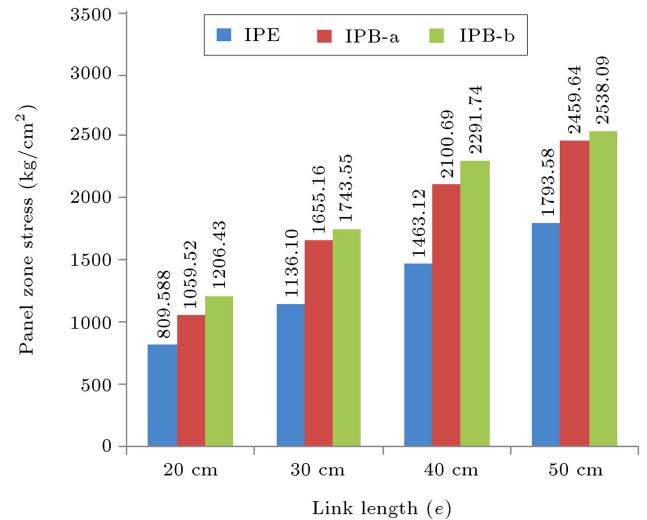


Figure 12. Maximum amounts of Von Mises stress in the V-EBF specimens panel zone.

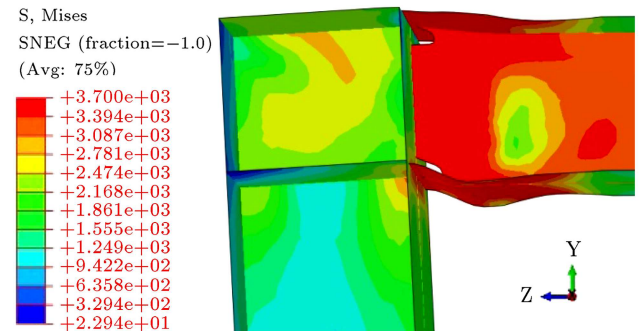


Figure 13. Von Mises stress distribution in S-7-1 model.

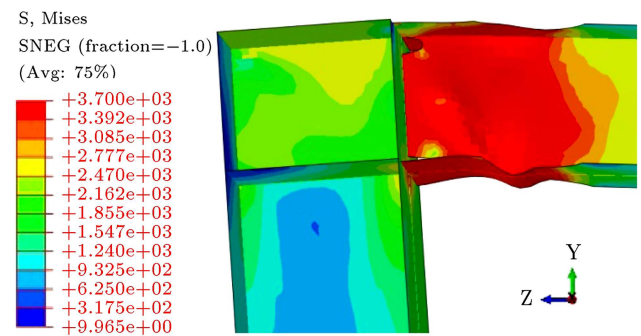


Figure 14. Von Mises stress distribution in S-7-4 model.

region of the beam adjacent to the column face, and the panel zone stress.

Figure 15 represents the maximum amount of Von Mises stress in the column panel zone of the SMRF specimens. It is observed that the value of stress in the panel zone of the first group of models (S-7 series) does not change significantly by an increase in the RBS-cut depth. But this value is considerably reduced by the increase in the amount of RBS-cut depth for the two other groups (S-12 and S-20 series). Thus, it is seen that in the RBS-cut depth values of 20% and 25%

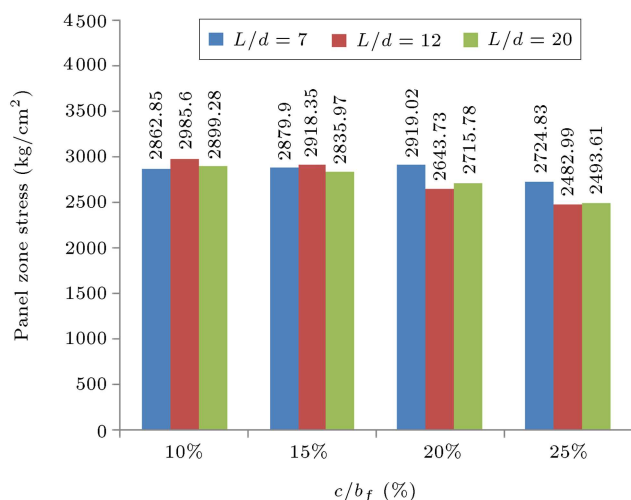


Figure 15. Maximum amounts of Von Mises stress in the SMRF specimens panel zone.

(deep RBS-cuts), the amounts of maximum stress in the panel zones of these two series are lower than that of the S-7 series.

4.2. Hysteresis curves

Hysteresis curves of the V-EBF models are presented in Table 4. The vertical axis is the base shear of the specimen (Ton), and the horizontal axis states its drift (the displacement measured on the upper story level divided by the height of the story). It is observed

that the V-EBF models have stable and complete cycles (without any geometric instability).

Hysteresis curves of the SMRF models are shown in Table 5. In these diagrams, the vertical axis expresses the base shear of the specimen (in Ton), and the horizontal axis represents the “Rotation” or “Drift” (the horizontal displacement of the top story in the loading direction of the specimen divided by its height) of the specimen. It can be seen that the hysteresis curves of some of the specimens are a little unstable. Indeed, in some of the specimens, lateral-torsional buckling (geometric instability) is observed.

4.3. Ductility

The value of ductility (μ) is defined by Eq. (12) [26]:

$$\mu = \Delta_m / \Delta_y, \quad (12)$$

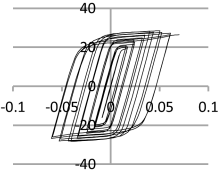
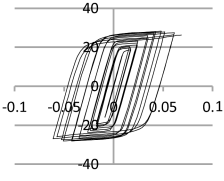
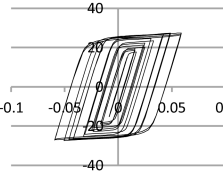
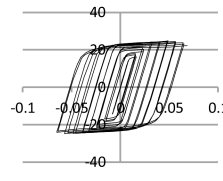
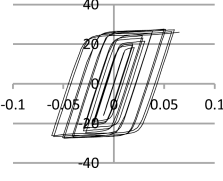
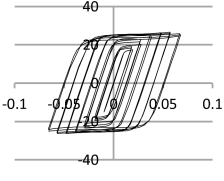
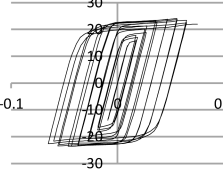
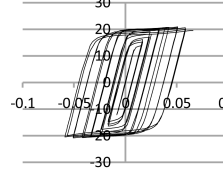
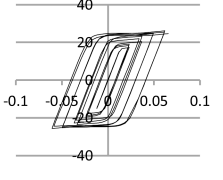
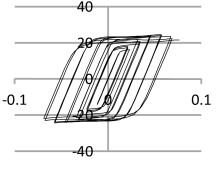
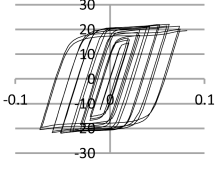
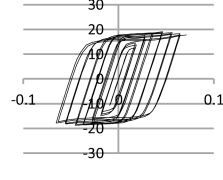
where Δ_m and Δ_y are the maximum amounts of displacement and yield displacement, respectively.

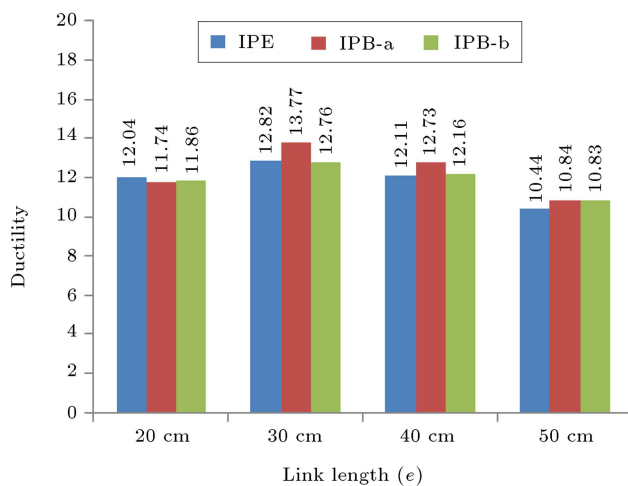
The ductility capacities of the V-EBF models are compared in Figure 16. The models are classified in three groups, as expressed earlier. It can be clearly seen that all three groups follow the same pattern of evolution. First, by increasing the value of link length, the ductility ratios of these three groups of V-EBF models increase, and in the length of 30 cm, they grasp their maximum values. However, after this point, the rates of slope go down and minimum values

Table 4. The hysteresis curves of V-EBF models.

S1	S2	S3	S4
S5	S6	S7	S8
S9	S10	S11	S12

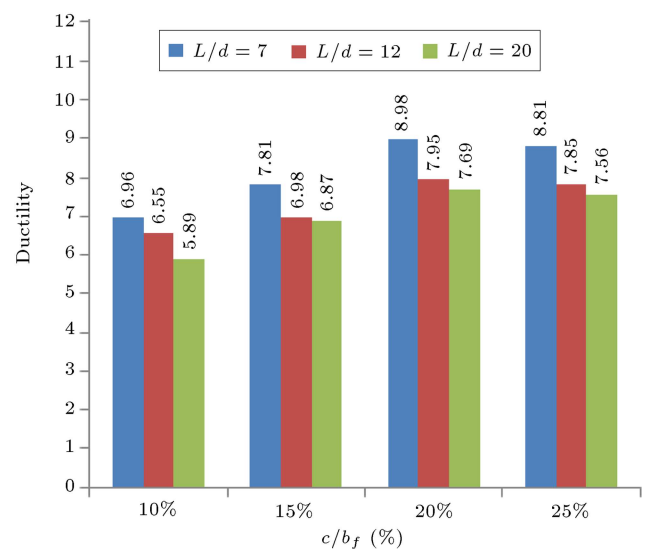
Table 5. The hysteresis curves of SMRF models.

S-7-1	S-7-2	S-7-3	S-7-4
			
S-12-1	S-12-2	S-12-3	S-12-4
			
S-20-1	S-20-2	S-20-3	S-20-4
			

**Figure 16.** Ductility ratios of the V-EBF models.

are obtained at a length of 50 cm. In addition, it is observed that, except for the link length of 20 cm, the second group (IPB-a) has the maximum values of ductility ratio, and gets to the maximum value of ductility at a link length of 30 cm, with a value of 13.77.

The ductility ratios of the SMRF models are compared in Figure 17. It is observed that by increasing the ratio of RBS-cut depth, the ductility ratios of all three groups increase, and reach their maximum amounts at the RBS-cut depth of 20%. After this, they almost

**Figure 17.** Ductility ratios of the SMRF models.

remain the same (with a small reduction). In addition, as this bar chart shows, the first group (S-7 series) has the maximum values of ductility ratio and grasps the maximum value of 9.98 in the RBS-cut depth equal to 30 cm. After that, the second and third groups (S-12 and S-20 series, respectively) are located in the second and third places, respectively. Furthermore, comparing Figures 16 and 17, it is found that the maximum ductility ratio of V-EBF models (13.77) is

about 1.4 times more than that of the SMRF models (9.98).

4.4. Energy dissipation capacity

For the purpose of investigating how much of the internal energy (total strain energy) of each sample is dissipated by plastic deformation, in this research, a new criterion is defined: the “*Dissipation Factor*” (DF), which is calculated by the following relation:

$$DF = \frac{E_P}{E_I}, \quad (13)$$

where E_P and E_I are the energy dissipated by plasticity, and the internal energy, respectively. The value of E_I can be evaluated by the following equation [27]:

$$E_I = E_S + E_P + E_C, \quad (14)$$

where E_S and E_C are the applied elastic strain energy, and the energy dissipated by time-dependent deformation (creep, swelling, and viscoelasticity), respectively.

Diagrams of the internal energy (E_I) and the energy dissipated by plastic deformations (E_P) are illustrated in Figure 18. The ultimate values of E_I and E_P of specimen S1 are equal to 11.8 (Ton.m) and 5.13 (Ton.m), respectively. So, the value of DF calculated by Eq. (13) is equal to 0.44, which means that 44% of the internal energy of specimen S1 is dissipated by plastic deformations.

Similarly, the DF values of all the V-EBFs are represented in Figure 19. It can be seen clearly that the first group (IPE) has the maximum values of DF, which are almost the same (equal to 43%). The second and third groups (with IPB link sections) have almost the same values of DF (near to 30%).

The DF values of all the SMRFs are represented in Figure 20. It can be seen that, except for specimen S-20-1 with the RBS-cut ratio of 10% (in which formation of the plastic hinges in the RBS regions had some trouble), evolution of the RBS-cut ratio has no significant effect on the value of DF. However, increase

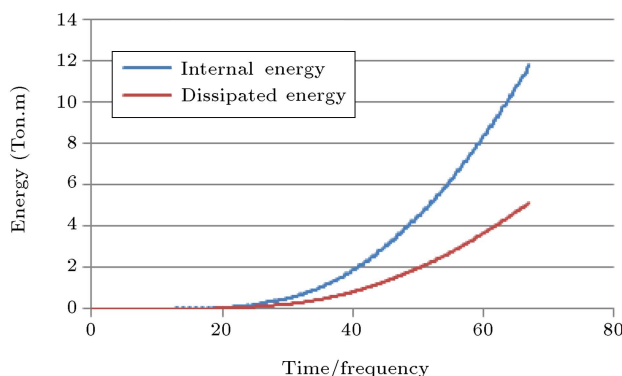


Figure 18. The diagrams of the internal energy and the energy dissipated by plastic deformations.

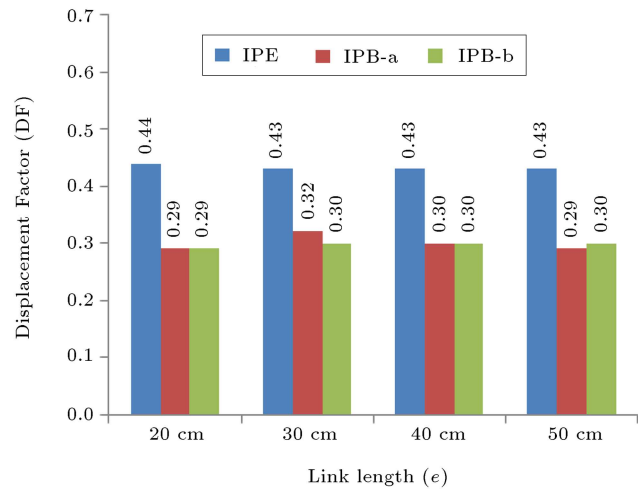


Figure 19. The DF values of all the V-EBFs.

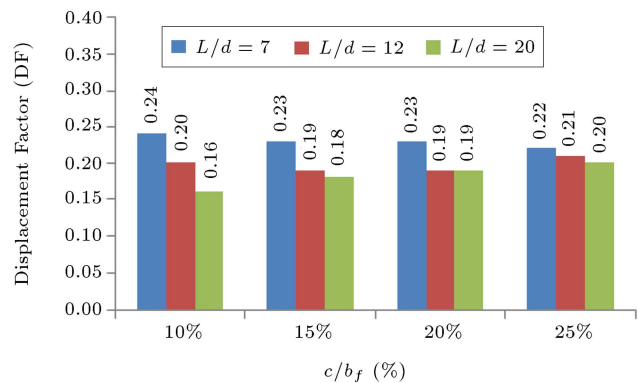


Figure 20. The DF values of all the SMRFs.

of the clear span-to-beam depth ratio leads to a smooth reduction in the DF value. It is observed that the first, second and third groups of specimens (S-7, S-12, and S-20 series) have almost average DF values of 23%, 20%, and 18%, respectively. Also, by comparing the maximum DF value of the V-EBFs (0.44) with that of the SMRFs (0.24), it is found that the dissipation capacity of the V-EBF is about 1.4 times more than the dissipation capacity of the SMRF.

5. Conclusions

In this paper, the ductility and energy dissipation capacities of Eccentrically Braced Frames with vertical link beams (V-EBFs) and Special Moment Resisting Frames (SMRFs) are investigated and the results show that:

1. The increase of link length in V-EBFs results in:
 - Increase of the stress value in the beam web panel zone.
 - Increase of the ductility ratio till a link length of 30 cm and, after this point, reduction of this value.

- No significant evolution of the energy dissipation capacity.
2. By comparing the results of specimens with IPE link sections, with those of the IPB, it is found that:
 - Links with IPE sections produce significantly less Von Mises stress values in the beam web panel zones.
 - In small values of link length (till a link length of 20 cm), links with IPE sections have more ductility ratios. However, after this point, the links with IPB sections grasp more ductility ratios.
 - Links with IPE sections have more energy dissipation capacities.
 3. Comparing the second group of specimens (IPB-a), with the third (IPB-b), which is constructed of the same link sections and just differs in the number of stiffeners, it can be found that the increase in stiffeners (more than the minimum required), results in:
 - Increase of the stress value of the beam web panel zone.
 - Almost, reduction of the ductility ratio.
 - No significant evolution of the energy dissipation capacity.
 4. The increase in RBS-cut depth ratio in SMRFs results in:
 - Reduction of the stress value of the beam web panel zone in most cases.
 - Increase in the ductility ratio till the RBS-cut depth ratio of 20% and, after this point, reduction of this value.
 - No significant evolution of the energy dissipation capacity, in most cases.
 5. The increase in span-to-beam depth ratio in SMRFs results in:
 - No considerable changes in the value of beam web panel zone stress, in the small amounts of RBS-cut depth ratios (till 15%), however, there is a reduction of this value for major amounts of RBS-cut ratios (20% and 25%).
 - Reduction of the energy dissipation capacity.
 6. The ductility and energy dissipation capacity of the V-EBF system is almost 1.4 times more than that of the SMRF system.

References

1. Roeder, C.W. and Popov, E.P. "Eccentrically braced steel frames for earthquakes", *Journal of the Structural Division*, **104**(3), pp. 391-412 (1978).
2. Roeder, C.W. and Popov, E.P. "Cyclic shear yielding of wide-flange beams", *Journal of the Engineering Mechanics Division*, **104**(4), pp. 763-80 (1978).
3. Popov, E.P. and Bertero, V.V. "Seismic analysis of some steel building frames", *Journal of the Engineering Mechanics Division*, **106**(1), pp. 75-92 (1980).
4. Hjelmstad, K.D. and Popov, E.P. "Cyclic behavior and design of link beams", *Journal of Structural Engineering*, **109**(10), pp. 387-403 (1983).
5. Hjelmstad, K.D. and Popov, E.P. "Characteristics of eccentrically braced frames", *Journal of Structural Engineering*, **110**(2), pp. 340-53 (1984).
6. Berman, J.W. and Bruneau, M., *Further Development of Tubular Eccentrically Braced Frame Links for the Seismic Retrofit of Braced Steel Truss Bridge Piers*, Technical Report MCEER 06-0006, Multidisciplinary Center for Earthquake Engineering Research, Buffalo, NY (2006).
7. Berman, J.W. and Bruneau, M. "Experimental and analytical investigation of tubular links for eccentrically braced frames", *Engineering Structures*, **29**(8), pp. 1929-1938 (2007).
8. Berman, J.W. and Bruneau, M. "Tubular links for eccentrically braced frames, Part 1: Finite element parametric study", *Journal of Structural Engineering*, **134**(5), pp. 692-701 (2008a).
9. Berman, J.W. and Bruneau, M. "Tubular links for eccentrically braced frames. Part 2: Experimental verification", *Journal of Structural Engineering*, **134**(5), pp. 702-712 (2008b).
10. AISC, *Seismic Provisions for Structural Steel Buildings*, AISC/ANSI 341-10, American Institute of Steel Construction, Chicago, IL (2010).
11. Wakabayashi, M., *Steel Structure*, Maruzen, Tokyo, Japan, pp. 399-403 (1989).
12. Fehling, E., Pauli, W. and Bouwkamp, J.G. "Use of vertical shear-links in eccentrically brace frames", In *Earthquake Engineering*, 10th World Conference, Balkema, Rotterdam (1992).
13. Astaneh-Asl, A. "Seismic design of special concentrically braced steel frames", *Steel Tips*, Structural Steel Educational Council (SSEC), Berkeley, California (1995).
14. Astaneh-Asl, A. "Cyclic tests and seismic design of steel gusset plates in buildings", in *Proceedings of the 3rd International Conference on Seismology and Earthquake Engineering (SEE3)*, Tehran, I.R. Iran (1999).
15. Sarraf, M. and Bruneau, M. "Ductile seismic retrofit of steel deck-truss steel bridges. 2: Design applications", *Journal of Structural Engineering*, **124**, pp. 1263-1271 (1998).
16. Bruneau, M. and Sarraf, M. "Innovative application of ductile system in seismic retrofit of deck-truss bridges", in *12th World Conference on Earthquake Engineering* (2000).

17. Sarraf, M. and Bruneau, M. "Performance tests of innovative ductile steel retrofitted deck-truss bridges", in *13th World Conference on Earthquake Engineering*, Vancouver, B.C., Canada, August, pp. 1-6 (2004).
18. Zahrai, M. and Bruneau, M. "Ductile end-diaphragms for seismic retrofit of slab-on-girder steel bridges", *Journal of Structural Engineering*, **125**, pp. 71-80 (1999).
19. Zahrai, M. and Bruneau, M. "Cyclic testing of ductile end diaphragms for slab-on-girder steel bridges", *Journal of Structural Engineering*, **125**, pp. 987-996 (1999).
20. ADINA, R and D, Inc. "Automatic dynamic incremental nonlinear analysis", *ADINA Software and Documentations*, ADINA, Watertown, Mass (1995).
21. Prakash, V., Powell, G.H. and Campbell, C. "DRAIN-2DX base program description and user guide", Rep. No. UCB/SEMM 93/17, University of California, Berkeley, California (1993).
22. ABAQUS, *ABAQUS Finite Element Analysis*, V-6.12.1, United States of America (2012).
23. AISC, *Prequalified Connections for Special and Intermediate Steel Moment Frames for Seismic Applications*, American Institute of Steel Construction, Chicago, Illinois, pp. 60601-1802 (2010).
24. AISC, *Specification for Structural Steel Buildings*, AISC/ANSI 360-05, American Institute of Steel Construction, Inc., Chicago, IL (2010).
25. ATC, *Guidelines for Cyclic Seismic Testing of Components of Steel Structures*, ATC-24, Applied Technology Council, Redwood City, CA (1992).
26. Azhari, M. and Mirghaderi, R., *Design of Steel Structures*, **4** (Seismic Design Issues), 2nd Ed, Arkan-e-Danesh Press, Isfahan, I.R. Iran (in Persian) (2011).
27. HKS, *ABAQUS Standard User Manual*, Version 6.12.1, Hibbitt, Karlsson, and Sorensen, Inc., Providence (RI) (2012).

Biographies

Saeid Pourzeynali received his MS degree in Structural Engineering, in 1989, from Tehran University, Iran, and joined the University of Guilan, Rasht, Iran, as lecturer in the Department of Civil Engineering. In 1991, Dr. Pourzeynali obtained his PhD degree in Structural Engineering from IIT Delhi, India, and is currently at the University of Guilan, Iran. His research interests span a wide range of specialized fields, including structural dynamics, earthquake engineering, random vibrations, reliability analysis, structural control and optimization, and dynamics of cable supported bridges. Dr. Pourzeynali has more than 24 years experience in teaching and has supervised 30 MS degree students. He has published more than 90 international journal and conference papers, and has received various awards, including "best research study on cable supported bridges" in 2004 from the Vice-Chancellor for Research at the University of Guilan.

Ashkan Shakeri received his BS degree in Civil Engineering from Islamic Azad University, Bandar Anzali, Iran, in 2010, and his MS degree in Structural Engineering from the University of Guilan, Rasht, Iran, in 2013. His main research interests include steel structures, energy dissipation devices, finite elements, structural dynamics, fatigue, and crack mechanics. He has published a number of papers concerning steel structures.